Coordination of tumor growth and host wasting by tumor-derived Upd3

Guangming Ding[1,2,3,6], **Xiaoxiang Xiang**[1,2,3,6], **Yanhui Hu**[4,6], **Gen Xiao**[1,2,3], **Yuchen Chen**[1,2,3], **Richard Binari**[4], **Aram Comjean**[4], **Jiaying Li**[1,2,3], **Elisabeth Rushworth**[2], **Zhenming Fu**[3], **Stephanie E. Mohr**[4], **Norbert Perrimon**[4,5,*], **Wei Song**[1,2,3,7,*]

[1]Department of Hepatobiliary and Pancreatic Surgery, Zhongnan Hospital of Wuhan University, Wuhan, Hubei 430071, PR China

[2]Frontier Science Center for Immunology and Metabolism, Medical Research Institute, Wuhan University, Wuhan, Hubei 430071, PR China

[3]Department of Oncology, Renmin Hospital of Wuhan University, Wuhan, Hubei 430060, PR China

[4]Department of Genetics, Harvard Medical School, Boston, MA 02115, USA

[5]Howard Hughes Medical Institute, Boston, MA 02115, USA

[7]Lead contact

SUMMARY

yki-induced gut tumors in *Drosophila* are associated with host wasting, including muscle dysfunction, lipid loss, and hyperglycemia, a condition reminiscent of human cancer cachexia. We previously used this model to identify tumor-derived ligands that contribute to host wasting. To identify additional molecular networks involved in host-tumor interactions, we develop PathON, a web-based tool analyzing the major signaling pathways in *Drosophila*, and uncover the Upd3/Jak/Stat axis as an important modulator. We find that *yki*-gut tumors secrete Upd3 to promote self-overproliferation and enhance Jak/Stat signaling in host organs to cause wasting, including muscle dysfunction, lipid loss, and hyperglycemia. We further reveal that Upd3/Jak/Stat signaling in the host organs directly triggers the expression of *ImpL2*, an antagonistic binding protein for insulin-like peptides, to impair insulin signaling and energy balance. Altogether, our results demonstrate that *yki*-gut tumors produce a Jak/Stat pathway ligand, Upd3, that regulates both self-growth and host wasting.

In brief

Ding et al. show that yki^{3SA}-gut tumors produce Upd3 as a cachectic ligand to simultaneously promote self-growth and host organ wasting via systemic activation of Jak/Stat signaling in *Drosophila*. The Upd3/Jak/Stat axis induces host ImpL2 production and perturbs insulin response, leading to muscle mitochondrial dysfunction, lipid loss, and carbohydrate elevation.

Graphical abstract
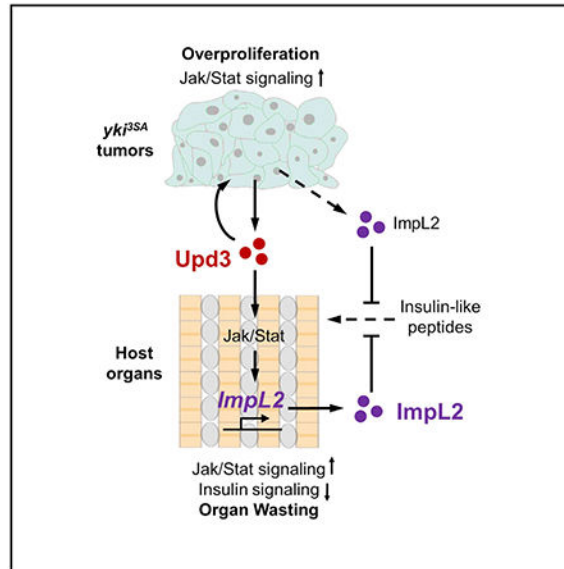
INTRODUCTION

Tumor-induced host organ wasting is a general phenomenon observed in both vertebrates and invertebrates. Patients with advanced cancers frequently develop severe organ wasting, referred to as "cancer cachexia," including muscle dysfunction, lipid loss, and hyperglycemia. Organ wasting is associated with resistance to chemotherapy, reduced quality of life, and mortality among patients with cancer (Fearon et al., 2013). Recent studies based on cultured cells and tumor-bearing mice have implicated a number of tumor-secreted cachectic proteins (e.g., PTHrP, activins, LIF, IL-6, and Hsp70/90), which remotely crosstalk to muscle and adipose tissues and modulate their metabolic homeostasis. In support of their roles, antibody neutralization of some of these proteins has been shown to improve organ wasting and survival of tumor-bearing subjects (Hirata et al., 2013; Kandarian et al., 2018; Kir et al., 2014; Zhang et al., 2017; Zhou et al., 2010). Despite these advances, however, there remains a need for genetic animal models that facilitate comprehensive evaluation of tumor-secreted proteins, associated signaling pathways, and their effects in host organs.

Drosophila is emerging as an excellent model to decipher the molecular mechanisms of tumor-induced host wasting. For example, aberrant activation of yki^{3SA}, a homolog of the human oncogene *YAP1*, in intestinal stem cells (ISCs) results in severe tumor cell overproliferation in the gut and subsequent muscle dysfunction, lipid loss, and

hyperglycemia (Kwon et al., 2015). Similar host wasting effects were also reported in other fly tumor models (Figueroa-Clarevega and Bilder, 2015; Katheder et al., 2017; Newton et al., 2020; Nie et al., 2019). As there is no evidence of metastasis from yki^{3SA}-gut tumors, a likely explanation is that host wasting is caused by tumor-secreted proteins that act remotely on host tissues. Previously, we identified two tumor-secreted proteins, the insulin-like polypeptide binding protein ImpL2 and the Pvr receptor tyrosine kinase ligand Pvf1, that impair the anabolism/catabolism balance of host organs (Kwon et al., 2015; Song et al., 2019). However, removal of either ImpL2 or Pvf1 from yki^{3SA} tumors only partially alleviates host wasting, suggesting that additional secreted proteins are involved in tumor-host interactions. Moreover, despite the impacts of tumor-derived ImpL2 and Pvf1 on host organs, they fail to affect growth of the gut tumor. Whether and how tumor-secreted ligands coordinate host wasting and tumor growth remain unclear.

Hormone/ligand-induced signaling plays a major role in interorgan communication. Classically, hormones/ligands trigger specific intracellular signaling pathways, including via activation of receptors, kinases/phosphatases, and transcriptional factors, and eventually regulate downstream gene expression. For example, the Unpaired 1, 2, and 3 (Upd1/2/3) ligands bind to their common receptor Dome and activate downstream kinase Jak/Hop and transcriptional factor Stat92E to regulate expression of Stat target genes such as *Socs36E* and *Dome* (Herrera and Bach, 2019). Thus, monitoring ligand expression in a sending organ and signature target gene expression of associated signaling pathways in a receiving organ can help identify the secreted ligands and corresponding signal reception and transduction pathways involved in interorgan communication.

In this study, we developed PathON, a web-based tool for analysis of ligands, signaling components, and signature target genes for 14 common canonical *Drosophila* signaling pathways: EGFR/FGFR/PvR, Hedgehog, Hippo, insulin, Jak/Stat, NF-κB/Imd, and NF-κB/Toll, Notch, TGF-β/BMP and TGF-β/Activin, TNF-α, and Wnt. We found that Jak/Stat signaling participates in tumor-host interactions. Combining genetic and molecular assays, we demonstrate that yki^{3SA}-tumor-derived Upd3 promotes both tumor growth and host wasting, including muscle dysfunction, lipid loss, and hyperglycemia, via systemic activation of Jak/Stat signaling. The results demonstrate that Upd3 acts as a tumor-secreted ligand that affects both tumor growth and host wasting.

RESULTS

Potential signaling pathways involved in tumor-host crosstalk

To develop PathON (https://www.fiyrnai.org/tools/pathon/web), we compiled a list of ligands (agonists and antagonists) and signaling components (receptors, kinases/phosphatases, adaptor proteins, and transcriptional factors) for 14 canonical *Drosophila* signaling pathways on the basis of the published literature (Table S1). Signature target genes for these pathways were selected if they had been previously validated by more than two of the following criteria: physiological function, gene expression, promoter activity, and direct binding to transcriptional factor(s) (Table S2).

On the basis of our hypothesis that *yki*-induced gut tumors produce specific ligands that activate associated signaling pathways and induce target gene expression in host organs, we applied PathON to analyze the expression levels of ligands and signature target genes of 14 signaling pathways in published RNA sequencing (RNA-seq) datasets from yki^{3SA}-tumor guts (GSE113728) and muscles (GSE65325) of yki^{3SA}-tumor-bearing files. Interestingly, a Jak/Stat signaling ligand (*upd3*, 37-fold induction) is one of the top genes upregulated in yki^{3SA}-tumor guts (Figure 1A). Signature target genes of Jak/Stat signaling are also significantly enriched among differentially expressed genes in the muscles of yki^{3SA}-tumor-bearing files (Figure 1A). Together, this suggests that Upd3 from yki^{3SA}-gut tumors activates Jak/Stat signaling in muscles.

We note that the ligands of insulin (*ImpL2*, 58-fold induction; and *Ilp3*, 2.5-fold induction), PvR (*Pvf2*, 20-fold; *Pvf1*, 14-fold), EGFR (*aos*, 8-fold; *spi*, 4-fold; *vn*, 3.5-fold; *Krn*, 2.6-fold), Hedgehog (*hh*, 7-fold), TGF-β/BMP (*cv-2*, 6-fold; *sog*, 4-fold; *gbb*, 2.5-fold; *cv*, 2.2-fold), Wnt (*Wnt5*, 6-fold and *Wnt6*, 1.8-fold), Notch (*Dl*, 5-fold), and TNF-α (*egr*, 2.5-fold) signaling pathways are also significantly increased in yki^{3SA}-tumor guts (Figure 1A). In addition, signature target genes of TGF-β/BMP, NF-κB/Imd, NF-κB/Toll, insulin, EGFR/FGFR/PvR, and TNF-α signaling pathways are significantly enriched among differentially expressed genes in the muscles of tumor-bearing fiies (Figure 1A). As we previously analyzed the roles of ImpL2 and Pvf1 in tumor-host interaction (Kwon et al., 2015; Song et al., 2019), we decided to focus on *upd3*, the second most increased ligand, and its associated Jak/Stat signaling pathway.

We first examined the target genes of Jak/Stat signaling and found that the transcriptional levels of most of these genes were significantly changed in the muscles of yki^{3SA}-tumor-bearing fiies, as indicated by RNA-seq (Figure 1B; Figure S1). For example, *Socs36E* was robustly increased. Upregulation of *Socs36E* in this context was further validated by qPCR (Figure 1C). We also examined activation of Jak/Stat signaling in the muscles of yki^{3SA}-tumor-bearing files using reporter assays. To do this, either control or yki^{3SA} files without GFP labeling in ISCs were crossed to *10XStat-GFP* reporter lines. The muscles from yki^{3SA} files exhibited abnormal myofibril morphology, and more Stat-GFP accumulated in the space between myofibrils and nuclei compared with control (Figure 1D), confirming that muscle Jak/Stat signaling is enhanced. Stat-GFP signaling was also increased in the fat body and in tumor-bearing guts in yki^{3SA} files (Figure 1D).

We next validated ligand induction in yki^{3SA}-gut tumors. The transcriptional level of *upd3*, but not *upd1* or *upd2*, was dramatically increased in tumors, as revealed by RNA-seq (>20-fold; Figure 1E). This result was further confirmed using qPCR, *upd3-LacZ* reporter, and MARCM clones (Figures 1F–1H). Altogether, the changes in transcription of the Jak/Stat ligand *upd3* in yki^{3SA}-gut tumors and of Jak/Stat target genes in muscles suggest that Upd3/Jak/Stat signaling is involved in tumor-host interactions.

Upd3 is essential for yki^{3SA}-gut tumor growth

To test whether yki^{3SA}-tumor-derived Upd3 directly regulates host wasting, we knocked down *upd3* expression specifically in yki^{3SA} tumors. Interestingly, the growth of yki^{3SA}-gut tumors and *Socs36E* expression indicating Jak/Stat pathway activity in the muscle were

potently suppressed under these conditions (Figure 1I; Figure S2A). Consistent with this result, the growth of yki^{3SA}-gut tumors in $upd3$ mutant files was also diminished (Figure S2B). Previous studies have indicated that Upd3 triggers Jak/Stat signaling in ISCs to promote proliferation in response to tissue damage and infection (Shaw et al., 2010). We found that knockdown of *dome, hop* (Jak), or *Stat92E* (Stat) in yki^{3SA}-gut tumors also suppressed tumor growth (Figure 1I). Taken together, our results show that yki^{3SA} tumors produce Upd3 and activate Jak/Stat signaling to promote self-growth in an autocrine/paracrine manner.

Tumor-derived Upd3 is essential for host wasting

To investigate the role of Upd3 in tumor-induced host wasting, we expressed a constitutively active form of hop (hop^{TumL}) in yki^{3SA}-gut tumors, creating a situation in which Jak/Stat signaling and tumor growth are sustained independent of extracellular Upd3, and then removed tumor-derived $upd3$ (Figure 2A). Consistently, compared with flies bearing either yki^{3SA} or $yki^{3SA}+hop^{TumL}$ gut tumors, specific $upd3$ knockdown in $yki^{3SA}+hop^{TumL}$ tumors using two different RNAi lines no longer suppressed tumor growth (Figure 2B; Figure S2C). Strikingly, removal of $upd3$ in $yki^{3SA}+hop^{TumL}$ tumors sufficiently alleviated the effects of systemic wasting, including the bloating phenotype, reduction in TAG levels, elevation of carbohydrate levels, and decreased climbing ability (Figures 2B–2D and 3A; Figures S2C and S2D). We note that removal of $upd3$ from $yki^{3SA}+hop^{TumL}$ tumors does not affect the expression levels of *ImpL2* or *Pvf1*, two previously identified tumor-derived cachectic ligands (Figure 2E).

We also asked whether inhibition of Upd3/Jak/Stat signaling in host organ tissues is sufficient to suppress tumor-induced wasting. To do this, we fed yki^{3SA}-gut tumor flies methotrexate (MTX), a potent small-molecule inhibitor of Jak/Stat signaling (Thomas et al., 2015), simultaneously with yki^{3SA}-tumor induction and found that treatment with 10 or 100 μM MTX strongly suppressed Jak/Stat signaling in both host organs and yki^{3SA}-gut tumor and decreased tumor growth at day 8 of tumor induction (Figures S3A and S3B). In order to reduce the impact of the drug on tumors and investigate its roles in host organs, we constitutively enhanced Jak/Stat signaling in yki^{3SA} tumors by inducing hop^{TumL} and decreased the MTX dose. Interestingly, although treatment with 0.1 or 1 μM MTX rarely suppressed the growth of $yki^{3SA}+hop^{TumL}$ tumors, it significantly reduced bloating and improved wasting effects, including climbing defects, lipid loss, and hyperglycemia (Figures S3C and S3D). These results collectively indicate that gut tumor-derived Upd3 acts remotely to induce Jak/Stat signaling in host organs, resulting in bloating/wasting.

Upd3/Jak/Stat signaling perturbs muscle mitochondrial homeostasis

As $upd3$ removal from yki^{3SA} tumors significantly restored fly climbing rates (Figure 3A), we asked how tumor-derived Upd3 regulates muscle function. We first investigated muscle mitochondrial activity, which has been shown to be remotely impaired by yki^{3SA}-gut tumors (Kwon et al., 2015). As expected, transmission electron microscopy (TEM) revealed normal mitochondrial integrity (M) in control muscles. In contrast, we observed swelling mitochondria with fragmented cristae (C) and low-density inner space (S) in the muscles of flies bearing yki^{3SA}-tumors, suggesting a classic degenerative phenotype

of mitochondria (Figure 3B). Flies bearing $yki^{3SA}+hop^{TumL}$ tumors exhibited severer mitochondrial degeneration, as indicated by the absence of cristae and blank inner space (S) in the muscle (Figure 3B). Strikingly, $upd3$ removal in $yki^{3SA}+hop^{TumL}$ tumors robustly eliminated mitochondrial degeneration and restored mitochondrial morphology, almost to control levels (Figure 3B). Moreover, $upd3$ knockdown in $yki^{3SA}+hop^{TumL}$ tumors also increased muscle ATP production, another important indicator of mitochondrial dysfunction (Figure 3C).

We next wondered whether Upd3/Jak/Stat signaling directly impairs muscle function. To address this, we genetically activated Jak/Stat signaling in adult muscles via hop^{TumL} overexpression driven by *Mhc-GAL4*. Interestingly, obvious morphological changes indicative of mitochondrial degeneration was observed in adult muscle (Figure 3D). Muscle ATP production was also decreased and fly climbing ability was impaired (Figures 3E and 3F). These results were further confirmed using another temperature-sensitive muscle driver *tub-GAL80^{TS}; dMef2-GAL4* (*dMef2^{TS}*) (Figures 3E and 3F). Taken together, our results indicate that the Upd3/Jak/Stat cascade mediates tumor-induced muscle mitochondrial degeneration and muscle dysfunction.

Excessive ubiquitin-associated protein degradation has also been associated with tumor-induced muscle dysfunction with (Acharyya and Guttridge, 2007). In line with this observation, we observed an increase in protein ubiquitination in the muscles of yki^{3SA} flies (Figure S4A). However, neither $upd3$ knockdown in the $yki^{3SA}+hop^{TumL}$ tumors nor activation of Jak/Stat signaling in the wild-type adult muscle significantly affected ubiquitination of muscle proteins (Figure S4B). The expression level of *CG11658*, which encodes a fly homolog of Atrogin-1 E3 ubiquitin ligase, was significantly increased in the muscle of yki^{3SA} flies but not in hop^{TumL}-overexpressing muscle (Figure S4C), indicating that Upd3/Jak/Stat signaling does not increase ubiquitination of muscle proteins in *Drosophila*.

Upd3/Jak/Stat cascade impairs muscle insulin response

Insulin signaling has been shown to regulate mitochondrial homeostasis and muscle function across species (Del Campo et al., 2016). We therefore examined whether tumor-derived Upd3 remotely affects muscle through attenuation of the insulin response. We knocked down $upd3$ expression in $yki^{3SA}+hop^{TumL}$ gut tumors and as expected, we found a significant decrease in the expression level of the Jak/Stat pathway target gene *Socs36E* in the fly muscle (Figure 4A). Interestingly, expression levels in the muscle of *4EBP* and *InR*, two target genes negatively regulated by insulin signaling, were also significantly decreased (Figure 4A). Akt phosphorylation (pAkt), an important positive readout of insulin signaling, was increased in the fly muscle (Figure 4B). These results collectively indicate that $upd3$ removal in $yki^{3SA}+hop^{TumL}$ gut tumors remotely enhances muscle insulin signaling.

To investigate whether Jak/Stat signaling directly attenuates insulin signaling, we specifically expressed hop^{TumL} in the muscle to activate Jak/Stat signaling and observed a significant decrease in pAkt (Figure 4C, left). This result was further validated by *ex vivo* assays in which adult thoracic muscles were isolated and treated with recombinant human insulin. Compared with control thoraces that exhibit a robust increase in insulin-stimulated

pAkt, hop^{TumL} overexpression in thoraces potently blunted this effect (Figure 4C, right). Consistent with pAkt changes, hop^{TumL} overexpression increased muscle expression of *Socs36E*, as well as *4EBP* (Figure 4D, left). Genetic manipulation using the temperature-sensitive muscle driver $dMef2^{TS}$ also obtained similar results (Figure 4D, right), suggesting that Jak/Stat signaling autonomously suppresses insulin response in the muscle.

To investigate whether Jak/Stat signaling impairs muscle functions through attenuation of insulin response, we manually restored the insulin response by overexpressing a constitutively active form of the InR (InR^{AC}) in the muscle in the context of hop^{TumL}. As expected, *4EBP* expression in the muscle was dramatically suppressed (Figure 4E), indicating an increase of insulin signaling. Moreover, muscle mitochondrial degeneration/swelling and fly climbing defects associated with hop^{TumL} were also remarkably diminished (Figures 4F and 4G). Therefore, our results collectively demonstrate that production of Upd3 by yki^{3SA}-gut tumors remotely activates Jak/Stat signaling and impairs insulin response in muscles, causing mitochondrial degeneration and muscle dysfunction.

Upd3/Jak/Stat cascade impairs insulin signaling and carbolipid metabolism in the fat body

Our results have demonstrated that tumor-derived Upd3 not only affects muscles but also leads to systemic lipid loss and carbohydrate elevation (Figure 2D), two additional major features of wasting. To investigate whether Upd3/Jak/Stat cascade directly affects the function of the fat body, the major metabolic organ in *Drosophila*, we activated Jak/Stat signaling specifically in the fat body. hop^{TumL} overexpression in wild-type adult fat body using the temperature-sensitive driver Cg-$GAL4$, tub-$GAL80^{TS}$ (Cg^{TS}) for 4 days robustly increased *Socs36E* mRNA levels in abdomens that contain large amounts of fat body cells (Figure S5A, left). Interestingly, fat-body hop^{TumL} overexpression significantly decreased TAG storage (Figure S5A, right). The abdominal fat layer potently disappeared in $Cg^{TS} > hop^{TumL}$ flies, so their abdomens appeared more translucent (Figure S5B, top). BODIPY staining also revealed that the lipid droplet mass in the fat body was dramatically reduced in $Cg^{TS} > hop^{TumL}$ flies (Figure S5B, bottom). Fat body hop^{TumL} overexpression using another driver, tub-$GAL80^{TS}$; Lpp-$GAL4$ (Lpp^{TS}), phenocopied systemic lipid loss in the abdomen (Figure S5C). In addition to lipid loss, fat-body hop^{TumL} overexpression also resulted in an elevated level of trehalose, the predominant insect circulating carbohydrate composed of two α-glucose, in $Cg^{TS} > hop^{TumL}$ flies (Figure S5A, right). Again, the metabolic imbalance was associated with impairment of the insulin response, which predominantly controls carbolipid metabolism in the fat body, as hop^{TumL} overexpression significantly elevated *4EBP* mRNA levels and decreased pAkt in the abdomen (Figure S5A, left; Figure S5D).

We have demonstrated that $yki3^{SA}$-gut tumors also secrete ImpL2, leading to wasting via antagonization of systemic insulin signaling (Kwon et al., 2015). As *upd3* removal in $yki^{3SA}+hop^{TumL}$ gut tumors does not affect *ImpL2* expression, we wondered whether tumor-derived ImpL2 and Upd3 are independent regulators. We knocked down both *ImpL2* and *upd3* in $yki^{3SA}+hop^{TumL}$ gut tumors to examine potential crosstalk. Interestingly, compared with knockdown of either *upd3* or *ImpL2*, knockdown of both ligands in $yki^{3SA}+hop^{TumL}$ tumors further alleviated wasting effects, including bloating rates and hyperglycemia, without affecting tumor growth (Figures S6A–S6D). Lipid loss was also improved but not

statistically significantly so (Figures S6A–S6D). Our results demonstrate that tumor-derived Upd3 and ImpL2 exhibit, at least, differential regulation of host wasting.

Upd3/Jak/Stat signaling induces *ImpL2* expression in the host organ

We next dissected the molecular mechanisms by which Jak/Stat signaling impairs the insulin response. To do this, we knocked down expression of *Stat92E*, the transcriptional factor of Jak/Stat signaling, in the context of hop^{TumL} overexpression in the muscle and, interestingly, observed an enhancement in pAkt levels and fly climbing ability (Figures S4D and S4E). The results suggest that Jak/Stat signaling might hamper insulin responses via Stat92E-dependent transcriptional regulation. Thus, we searched for potential Stat92E targets with the following three criteria: (1) known negative regulators of insulin signaling, (2) putative Stat-binding sites in the promoter regions, and (3) expression highly associated with Upd3/Jak/Stat signaling in the muscle. Our bioinformatic analysis identified *ImpL2* as a top candidate with four putative Stat-binding sites in its promoter region (BS1, BS2, BS3, and BS4) (Figure 5A). We further transfected Stat92E and Hop^{TumL} together with BS1–4 luciferase constructs in S2R$^+$ cells and found that BS2 luciferase activity was potently increased under these conditions (Figure 5B). We further mutated the two Stat-binding sites in BS2 region and, as expected, observed that BS2 luciferase activity was markedly blunted (Figure 5C). Chromatin immunoprecipitation (ChIP) assays also indicated that Stat92E specifically binds to the BS2 promoter region of *ImpL2* (Figure 5D). There results demonstrate that Stat92E is a major regulator of *ImpL2* expression that acts via a binding site in the BS2 region.

We next asked if Upd3/Jak/Stat signaling regulates *ImpL2* expression *in vivo* in the host organ. Our RNA-seq data (GSE65325) for yki^{3SA} flies showed a significant increase in *ImpL2* mRNA levels in the muscle (Figure 5E, left), a finding that correlates with upregulation of *upd3* production in yki^{3SA}-gut tumors and Jak/Stat signaling in the matched muscle (Figure 1). The result was also confirmed using qPCR (Figure 5E, right). Conversely, we specifically knocked down *upd3* expression in $yki^{3SA}+hop^{TumL}$ gut tumors, which significantly suppressed Jak/Stat signaling in the muscle (Figure 4A), and found that muscle *ImpL2* mRNA levels were dramatically decreased (Figure 5F). In order to study the autonomous regulation of Jak/Stat signaling on *ImpL2* expression, we activated Jak/Stat signaling by overexpressing hop^{TumL} in the muscle and observed a 3-fold induction of *ImpL2* mRNA levels in a Stat92E-dependent manner (Figure 5G). Thus, our data indicate that Upd3/Jak/Stat signaling transcriptionally regulates *ImpL2* expression in the muscle.

Upd3/Jak/Stat signaling causes host wasting in part via autonomous *ImpL2* expression

To examine whether Jak/Stat signaling impairs insulin response and muscle functions via autonomous ImpL2 production, we decreased *ImpL2* expression in the context of muscle hop^{TumL} overexpression. As expected, *ImpL2* RNAi in hop^{TumL}-overex pressing muscle dramatically decreased *ImpL2* mRNA level and also suppressed *4EBP* expression (Figure 6A), which reflects a restoration of the muscle insulin response. Furthermore, hop^{TumL}-associated mitochondrial degeneration in the muscle and fly climbing defects were both potently improved by *ImpL2* RNAi (Figures 6B and 6C).

Similar ImpL2 regulation by Jak/Stat signaling was also observed in the fat body. Overexpression of hop^{TumL} in the fat body resulted in an increase in *ImpL2* and *4EBP* mRNA levels, systemic TAG decline, and hyperglycemia (Figures 6D–6F), whereas *ImpL2* RNAi in the context of hop^{TumL} overexpression in the fat body diminished the effects associated with hop^{TumL} (Figures 6D–6F). Taken together, our results demonstrate that Upd3/Jak/Stat signaling increases autonomous ImpL2 production in the muscle and fat body to impair the insulin response and its associated energy balance.

Upd3 overexpression alone in ISCs sufficiently results in both tumor growth and host wasting

Finally, we asked whether Upd3 production alone in the gut is sufficient to cause host wasting. We overexpressed *upd3* in wild-type adult enterocytes (ECs) for 8 days and observed only mild ISC overproliferation (Figure S7A). However, the *Socs36E* and *4EBP* expression levels in the muscle were significantly increased (Figure S7B). EC-derived Upd3 production triggered host wasting, including lipid loss, carbohydrate elevation, and climbing defects (Figure S7C).

Furthermore, we overexpressed *upd3* in wild-type adult ISCs and observed the dramatic overgrowth of the GFP-labeled tumor cell population, expanding to the whole gut by 8 days (Figure 7A). As expected, *upd3*-induced gut tumors increased the expression levels of *Socs36E, ImpL2*, and *4EBP* in the muscle and triggered wasting effects, including muscle wasting, lipid loss, and carbohydrate elevation (Figures 7B–7D). However, we noted that Upd3 overexpression in either ECs or ISCs failed to trigger abdomen bloating and caused wasting effects not as severe as that observed with yki^{3SA}-induced gut tumors (Figures 7A and S7A). Taken together, our results indicate that Upd3 production alone in the gut sufficiently results in host wasting.

As Upd3/Jak/Stat signaling is required for ISC proliferation, we knocked down *Stat92E* or *dome* in the context of *upd3* overexpression in the ISCs and found that Upd3-induced tumor growth, host Jak/Stat activation, and host organ wasting were all remarkably suppressed (Figures S7D–S7F), suggesting that the mass of Upd3-producing cells is also important for host wasting regulation. We previously identified Pvf1 as an important tumor-derived cachectic ligand and wondered whether Pvf1 would synergize with Upd3 for host wasting. We overexpressed *Pvf1* in the wild-type adult ISCs and, consistent with previous studies (Bond and Foley, 2012), observed only mild ISC overproliferation (Figure S7G). Unexpectedly, we found that Pvf1 overexpression together with Upd3 antagonized Upd3-associated gut tumor formation and host wasting (Figure S7H), suggesting an unknown molecular mechanism(s) between Upd3 and Pvf1 regarding tumor-growth regulation in the gut.

DISCUSSION

The molecular mechanisms whereby malignant tumors coordinate self-growth and host organ wasting are not fully understood. In this study, which combined bioinformatics analysis and genetic validation, we identified tumor-derived Upd3 as an important mediator of tumor-host interaction. We demonstrate that tumor-derived Upd3 simultaneously activates

Jak/Stat signaling in gut tumor cells, promoting overgrowth of the tumor itself and, in host organs, causing energy imbalance and wasting.

PathON for evaluating signaling pathways involved in interorgan communication

We have demonstrated that monitoring signature target genes to evaluate the activity of various signaling pathways in a receiving tissue is helpful to comprehensively understand crosstalk networks during interorgan communication (Song et al., 2017b). One potential complication of this approach is that different pathways might share a set of common target genes. For example, both insulin and TNF-α signaling directly regulate *puc* expression (Bai et al., 2013; McEwen and Peifer, 2005). Moreover, the targets of a given pathway might also vary in different organs or at different developmental stages. Thus, we decided to evaluate enrichment of all potential target genes rather than single ones, and we developed the web-based analysis tool PathON to facilitate this approach. Using PathON, we successfully uncovered Upd3/Jak/Stat signaling pathway as an important mediator in the tumor-host crosstalk. It will be interesting to determine whether other pathways identified using PathON, such as the BMP and TNF-α signaling pathways, also play important roles in tumor-induced host wasting. In addition, we note that because we hypothesized that tumor-host interactions were mediated by signaling ligands, we focused on 14 canonical ligand-induced signaling pathways. Target genes of other pathways and transcriptional factors, such as hypoxia/HIF and circadian clock/Period, could be worth adding to PathON in the future to facilitate assessment of a more diverse set of biological processes.

Upd3 coordinates tumor growth and host wasting

How malignant tumors coordinate selfgrowth and host wasting is not fully understood. We have previously shown that yki^{3SA}-gut tumors produce ImpL2 to suppress systemic insulin availability and inhibit host anabolism (Kwon et al., 2015). We also found that yki^{3SA}-gut tumors constitutively activate intracellular insulin signaling, independent of circulating insulin-like peptides (ILPs), to overcome ImpL2-associated insulin insufficiency and growth restraint (Kwon et al., 2015; Lee et al., 2021). Moreover, the yki^{3SA} tumors also produce Vein (Vn) and Pvf1, which promote tumor growth and host wasting, respectively, through differential MEK activation in tumors and host organs (Song et al., 2019). Despite these various levels of regulation, here we document that Upd3 acts as a single tumor-derived ligand that simultaneously affects tumor growth and host wasting.

Upd3 is sufficient to mediate yki^{3SA}-gut tumor growth via activation of local Jak/Stat signaling in a paracrine/autocrine fashion, as many studies in fly ISCs models have indicated (Amoyel et al., 2014; Jiang et al., 2009; Katheder et al., 2017; Markstein et al., 2014; Ren et al., 2010; Shaw et al., 2010; Staley and Irvine, 2010). Meanwhile, the well-expanded yki^{3SA} tumors produce a large amount of Upd3, which has been characterized as a hormone (Huang et al., 2020; Woodcock et al., 2015), to activate Jak/Stat signaling in host organs and contributes to host wasting, including muscle dysfunction, lipid loss, and hyperglycemia. Consistent with this model, overexpression of *Upd3* alone in ISCs is sufficient to cause both gut tumors and host wasting. Because Yki has been shown to bind to the *upd3* promoter together with Sd to upregulate *upd3* transcription (Houtz et al., 2017), *upd3* induction in gut tumors is most likely directly regulated by Yki/Sd.

Upd3 has been considered a homolog of mammalian interleukins (ILs), which canonically activate Jak/Stat signaling and are highly associated with cancer cachexia and muscle wasting (Bonetto et al., 2012; Flint et al., 2016; Laird et al., 2021; Strass-mann et al., 1992). However, ILs are produced mostly in host organs, and the effects on muscle atrophy of different ILs, such as IL-1, IL-6, IL-8, and IL-12, remain controversial (Aoyagi et al., 2015), probably because of functional compensation and context-dependent differences. Using *Drosophila* as a conserved model organism with less gene redundancy, we demonstrate that tumor-derived Upd3 is sufficient and necessary to trigger host Jak/Stat signaling and cause wasting.

Upd3/Jak/Stat signaling impairs muscle function via mitochondrial degeneration rather than enhanced protein ubiquitination

The role of Upd3/Jak/Stat signaling in the *Drosophila* muscle is largely unknown. Mammalian Jak/Stat signaling has been shown to trigger muscle atrophy primarily through increased expression of E3 ubiquitin ligases (*Atrogin-1* and *MuRF1*) and enhanced protein ubiquitination to promote protein degradation (Sala and Sacco, 2016). However, in adult fly muscles, neither tumor-derived Upd3 nor autonomous Jak/Stat signaling increases protein ubiquitination. Moreover, Jak/Stat signaling in fly muscle also fails to increase the expression of *CG11658*, the homolog of Atrogin-1, further suggesting differences in regulation of Jak/Stat signaling in *Drosophila* compared with mammals. In this study, we showed that Upd3/Jak/Stat signaling in the muscle is sufficient to cause mitochondrial degeneration and leads to muscle dysfunction. The molecular mechanisms involve, at least, an impaired muscle insulin response. Thus, our study provides a novel understanding of Jak/Stat cascade in muscle physiology in *Drosophila* that could be a general biological process across species.

Besides tumor-derived ImpL2 and Upd3 that antagonize host insulin signaling to perturb muscle mitochondrial activity, we have previously shown tumor-derived Pvf1 as another modulator of muscle function via activating Pvr/MEK signaling to impair protein synthesis/breakdown balance (Kwon et al., 2015; Song et al., 2019). Taken together the fact that removal of *ImpL2, Pvf1* (Kwon et al., 2015; Song et al., 2019), or *upd3* in the gut tumors potently but not completely diminishes host wasting, we speculate that these tumor-derived cachectic ligands synergize to regulate host energy homeostasis. In the future, it will be interesting to further investigate the crosstalk and differential effects of these ligands in the host organs.

Upd3/Jak/Stat cascade inhibits muscle insulin signaling via cell-autonomous *ImpL2* induction

Several studies have indicated that activation of the Upd3/Jak/Stat cascade hampers the insulin response in various tissues (Kierdorf et al., 2020; Shin et al., 2020), although the molecular mechanisms underlying this observation are not well understood. In this study, we made the striking observation that Upd3/Jak/Stat signaling in host organs induces production of *ImpL2*, a well-known antagonist of both fly ILPs and human insulin/IGF (Sloth Andersen et al., 2000). This blocks extracellular ILPs and decreases the intracellular insulin response, resulting in mitochondrial degeneration and lipid loss. The results of our *in vitro* luciferase

assays further indicate that this occurs via Stat92E-dependent transcriptional regulation of *ImpL2*. Interestingly, our conclusion is also supported by the results of an earlier study revealing that expression of *ImpL2* is highly associated with expression of *Socs36E* and *Upd* genes in both testis and embryo (Terry et al., 2006). Mammalian Jak/Stat signaling has been reported to attenuate insulin signaling via SOCSs to degrade the insulin receptor and blunt phosphorylation of its downstream regulators (Jorgensen et al., 2013). *Drosophila* Socs36E functions as an important homolog of mammalian SOCSs and a negative regulator of multiple signaling pathways, including EGFR signaling, by degrading key components of these pathways (Amoyel et al., 2016; Stec et al., 2013). Thus, Socs36E might act together with ImpL2 to decrease intracellular insulin signaling.

Tumor-induced impairment of host insulin signaling is essential for systemic wasting. In our previous studies, we proposed that tumor-derived ImpL2 restrains the bioavailability of circulating ILPs and decreases muscle insulin responses (Figueroa-Clarevega and Bilder, 2015; Kwon et al., 2015). However, specific *ImpL2* removal in *yki^{3SA}*-gut tumors only moderately restores muscle insulin response compared with *ImpL2*-null mutation (Kwon et al., 2015), indicating that host organs also produce functional ImpL2 in addition to *yki^{3SA}*-gut tumors. Here, we show that ImpL2 production in the host organs, which is remotely induced by tumor-derived Upd3, also contributes to the impairment of insulin response and host wasting (Figure 7E).

STAR★METHODS

RESOURCE AVAILABILITY

Lead contact—Further information and requests for resources and reagents should be directed to and will be fulfilled by the lead contact, Wei Song (songw@whu.edu.cn).

Materials availability—All stable reagents generated in this study are available from the lead contact without restriction.

Data and code availability—This paper analyzes existing, publicly available data. These accession numbers for the datasets are listed in the key resources table. This paper does not report original code. Any additional information required to reanalyze the data reported in this paper is available from the lead contact upon request.

EXPERIMENTAL MODEL AND SUBJECT DETAILS

Fly strains—All flies, stocks and crosses, were grown under standard laboratory conditions (25°C, 12:12 h light/dark). to induce gut tumors, we followed the experimental procedures described previously (Song et al., 2019). Briefly, different *UAS* insertions were crossed to *esg-GAL4, tub-GAL80^{TS}, UAS-GFP* at 18°C to inactivate GAL4, thus restricting the expression of the Gal4-induced transgenes. 4-day-old adult progenies were collected and placed at 29°C to induce the transgenes (day 0 for tumor induction). Progenies from a cross between *esg-GAL4, tub-GAL80^{TS}, UAS-GFP* and *w^{1118}* or *UAS-w-RNAi* were used as controls. During incubation at 29°C, flies were transferred onto fresh food every 2 days.

For MARCM assays, we generated the progenies with indicated genotypes at 25°C. The 4-day old virgin adults were heat-shocked at 37°C for 30 min twice to induce gene expression and maintained back at 25°C for 6 days prior to midgut dissection and analysis.

METHOD DETAILS

Design and development of PathON—All ligands, signaling components (receptors, adaptor proteins, kinases and phosphatases, and transcriptional factors), and signature target genes for 14 signaling pathways were annotated from the published literature. Signature target genes for these pathways were selected only if they had been previously validated by more than two of the following criteria: physiological function, gene expression, promoter activity, or direct binding to transcriptional factor(s).

In many cases, ligands-induced signaling eventually leads to post-translational changes, like phosphorylation and ubiquitination, of signaling components and transcriptional changes of target genes. We integrated two RNA-seq datasets and focused on transcriptional expression of ligands in the yki^{3SA}-tumors and signature target genes in the muscle to evaluate the tumor-muscle signal crosstalk in this study. Because expression of signaling components and signature target genes is more context-dependent (e.g., different stages and tissues) than ligands, we evaluate them as a pool using Chi-square enrichment test. We also note that most of signature target genes for the PvR, EGFR, and FGFR signaling pathways overlap, and thus we grouped them together as targets of EGFR/FGFR/PvR signaling.

Lipid and carbohydrate measurements in flies—We measured fly TAG and carbohydrates as described previously (Song et al., 2017a; Song et al., 2017b; Song et al., 2010; Song et al., 2014). Briefly, 10 flies from each group were homogenized with 1 mL PBS containing 0.2% Triton X-100 using Multi-sample tissuelyser-24 (Shanghai Jingxin Technology) and heated at 70°C for 5 min. The supernatant was collected after centrifugation at 12,000 X g for 10 min at 4°C. 10 μL of supernatant was used for protein quantification using Bradford Reagent (Sigma, B6916-500ML). Whole body trehalose levels were measured from 10 μL of supernatant treated with 0.2 μL trehalase (Megazyme, E-TREH) at 37°C for 30 min using glucose assay reagent (Megazyme, K-GLUC) following the manufacturer's protocol. We subtracted the amount of free glucose from the measurement and then normalized the subtracted values to protein levels in the supernatant. To measure whole body triglyceride levels, we processed 10 μL of supernatant using a Serum Triglyceride Determination kit (Sigma, TR0100), subtracted the amount of free glycerol in the supernatant from the measurement, and then normalized to protein levels in the supernatant.

Climbing activity—Flies were placed in an empty vial and then tapped down to the bottom. They were allowed to climb for 3 s. Climbing was video recorded and climbing height and speed were calculated from the video. A minimum of 15 flies and 10 separate trials were performed for each condition.

Muscle ATP measurements—Five adult thoraces were freshly homogenized in 100 μL of PBS, immediately heated at 70°C for 5 min, and centrifuged at 12,000 Xg for 5 min

at 4°C to remove cuticle and cell debris. The supernatants were 1:500 diluted to measure the ATP levels using a CellTiter-Lumi™ Plus kit (Beyotime, C0068M). The final ATP production levels were normalized to protein levels that were measured using Bradford Reagent (Sigma, B6916-500ML) in the supernatant.

Immunostaining—Adult midguts were dissected in PBS and fixed for 15 min in PBS containing 4% paraformaldehyde. After fixation, the samples were washed with PBS containing 0.2% Triton X-100 (PBST)and blocked with 1% BSA in PBST. After incubation with primary antibodies anti-β-Gal (1:500, Promega, Z3781) overnight at 4°C. Midguts were washed and then incubated with Alexa fluorescence secondary antibody (1:1000, Thermo Fisher, A32742) and DAPI (1:1000, ThermoFisher, D1306) for 1 h at room temperature, washed, and mounted in Vectashield (Vector, H-1000). Adult midguts, thorax muscles, as well as abdomens containing fat bodies, were dissected in PBS and fixed for 15 min in PBS containing 4% paraformaldehyde. After fixation, the samples were washed with PBST, incubated with Bodipy 493/503 (1 μg/mL, Thermo Fisher, D3922), Phalloidin (1:1000, Thermo Fisher, A12381), or DAPI (1:1000) for 1 h at room temperature, washed, and mounted in Vectashield (Vector, H-1000). Images of fly appearances were performed on a Nikon SMZ18 or Nikon Eclipse Ts2 and confocal images were obtained using a Zeiss LSM880.

Western blotting—Ten adult thoraces or abdomens without ovaries were lysed in RIPA buffer (50 mM Tris-HCl [pH 7.5], 5 mM EDTA, 10 mM Na4P2O7, 100 mM NaF, 1 mM phenylmethylsulfonyl fluoride, 1 mM Na3VO4, 10 μg/ml aprotinin, 10 μg/ml leupeptin, 1% Nonidet P-40). Extracts were immunoblotted with indicated antibodies: rabbit anti-phospho-Akt (S473) (1:1000, Cell Signaling, 4060), mouse anti-polyubi-quitin (FK2) (1:1000, Enzo, BML-PW8810), α-tubulin (1:5000, Sigma, T5168).

qPCR—A total of 10 adult midguts, 5 whole adult flies, or 5 adult thoraces of each genotype and were lysed with Trizol (Thermo Fisher, 15596018) for RNA extraction and cDNA was transcribed using HiScript II Q RT Supermix (Vazyme, R222-01). qPCR was then performed using ChamQ SYBR qPCR Master Mix (Vazyme, Q311-03) on a CFX96 Real-Time System/C1000 Thermal Cycler (Bio-Rad). *Drosophila* gene expression was normalized to *RpL32*.

Electron microscopy—Adult thoraces were processed and analyzed in cross-section following standard protocols (Electron Microscopy Facility at Harvard Medical School; https://electron-microscopy.hms.harvard.edu). Briefly, thoraces were fixed in 0.1 M sodium cacodylate buffer (pH 7.4) containing 2.5% glutaraldehyde, 2% paraformaldehyde overnight. The fixed samples were washed in 0.1M cacodylate buffer, fixed again with 1% osmium tetroxide (OsO4) and 1.5% potassium ferrocyanide (KFeCN6) for 1 hour, and washed 3 times in water. Samples were incubated in 1% aqueous uranyl acetate for 1 hour and followed by 2 washes in water and subsequent dehydration in grades of alcohol. The samples were then put in propylene oxide for 1 hour and embedded in TAAB Epon (Marivac Canada Inc.). Ultrathin sections (about 60 nm) were cut on a Reichert Ultracut-S microtome, moved to copper grids, and then stained with lead citrate. Sections were examined in a JEOL

1200EX transmission electron microscope, and images were recorded with an AMT 2k CCD camera.

Pharmaceutical Jak/Stat inhibition in flies—For pharmaceutical inhibition of Jak/Stat signaling, flies were transferred to food containing methotrexate (Selleckchem, S1210) simultaneously with tumor induction at 29°C.

Cell culture, constructs, luciferase, and ChIP assays—*Stat92E-RB* and *hop^{TumL}* fragments were cloned from cDNAs of wild-type and *hop^{TumL}*-overexpressing flies, respectively, into the *pAc5.1* vector (ThermoFisher, V411020) at EcoRI and *Xho*I sites using the exonuclease-based DNA assembly method (Vazyme, C113-01). The hsp70 promoter was excised from the *pUAST* plasmid and inserted into the pGL3-basic Luciferase Reporter Vector (Promega, E1751) at the *Hind*III site. Different fragments (BS1, BS2, BS3, BS4) of *ImpL2* promoter were cloned from the genome of *w^{1118}* flies and inserted into the *pGL3-hsp70* vector at XhoI site.

For luciferase assays, *Drosophila* S2R^{+} cells were seeded into a 48-well plate at 25°C with Schneider's medium supplemented with 10% fetal bovine serum, then transfected with 15ng *pGL3-BS1, pGL3-BS2, pGL3-BS3, pGL3-BS4*, or mutant *pGL3-BS2* together with 60 ng *pAc-Stat92E-RB* and/or 15 ng *pAc-hop^{TumL}* and 5 ng *pAc-renilla* for 2 days using the Effectene reagent (QIAGEN, 301425). Next, S2R^{+} cells were washed with PBS and lysed for measurements of firefly and Renilla luciferase activities using the Dual-Luciferase Reporter Assay Reagent (Promega, E1910). Firefly luciferase activities were normalized to Renilla luciferase activities. All of the results were obtained from at least three independent experiments.

For ChIP assays, *Drosophila* S2R^{+} cells were transiently transfected with *pAc-HRV.FLAG.Stat92E.RB-T2A-hop^{TumL}.GFP* for 2 days using the Effectene and cross-linked with 1% formaldehyde for 20 min and quenched with 135 mM glycine for 15 min at 25°C. Cells were lysed and chromatins were sheared by sonication in a QSonica sonicator (QSonica, LLC, Q125) for 15 times (10 s ON and 50 s OFF, 40% Amplitude). After centrifugation at 13,200 rpm for 15 min at 4°C and lysate supernatant was adjusted into 1.3 mL TE buffer containing 1% Triton X-100, 0.1% DOC, proteinase inhibitor cocktails. 50 μL of chromatin solution was used as Input DNA. 1.2 mL chromatin solution was incubated with the beads (Pierce Protein A/G Magnetic Beads, 88803) that were preblocked using 0.2 mg/mL glycogen, 0.2 mg/mL BSA, 0.2 mg/mL tRNA for 2 hours and pretreated with 10 μL anti-FLAG antibodies (Genscript, A01868) for 2 h. The mixture was incubated with HRV 3C Protease (TaKaRa, 7360-1) at 22°C for 2 h and later incubated with 120 μL Elution Buffer overnight at 65°C. The input DNA and immunoprecipitated DNA samples were subjected to qPCR in CFX384 Touch Real-Time PCR Detection System (Bio-Rad Laboratories). A fragment in the CDS region of *Sam-S* that contains no Stat-binding sites was used as the negative control.

QUANTIFICATION AND STATISTICAL ANALYSIS

Data are presented as the mean ± SEM. Unpaired Student's t test and one-way ANOVA followed by post hoc test were performed to assess differences. A *p* value of < 0.05 was

considered statistically significant. All of the statistical details of experiments and p values can be found in the figure legends.

Supplementary Material

Refer to Web version on PubMed Central for supplementary material.

ACKNOWLEDGMENTS

REFERENCES

Acharyya S, and Guttridge DC, (2007). Cancer cachexia signaling pathways continue to emerge yet much still points to the proteasome. Clin. Cancer Res13, 1356–1361. [PubMed: 17332276]

Amoyel M, Anderson AM, and Bach EA, (2014). JAK/STAT pathway dysregulation in tumors: a Drosophila perspective. Semin. Cell Dev. Biol28, 96–103. [PubMed: 24685611]

Amoyel M, Anderson J, Suisse A, Glasner J, and Bach EA, (2016). Socs36E controls niche competition by repressing MAPK signaling in the Drosophila testis. PLoS Genet. 12, e1005815. [PubMed: 26807580]

Aoyagi T, Terracina KP, Raza A, Matsubara H, and Takabe K, (2015). Cancer cachexia, mechanism and treatment. World J. Gastrointest. Oncol7, 17–29. [PubMed: 25897346]

Bach EA, Ekas LA, Ayala-Camargo A, Flaherty MS, Lee H, Perrimon N, and Baeg GH, (2007). GFP reporters detect the activation of the Drosophila JAK/STAT pathway in vivo. Gene Expr. Patterns7, 323–331. [PubMed: 17008134]

Bai H, Kang P, Hernandez AM, and Tatar M, (2013). Activin signaling targeted by insulin/dFOXO regulates aging and muscle proteostasis in Drosophila. PLoS Genet. 9, e1003941. [PubMed: 24244197]

Bond D, and Foley E, (2012). Autocrine platelet-derived growth factor-vascular endothelial growth factor receptor-related (Pvr) pathway activity controls intestinal stem cell proliferation in the adult Drosophila midgut. J. Biol. Chem287, 27359–27370. [PubMed: 22722927]

Bonetto A, Aydogdu T, Jin X, Zhang Z, Zhan R, Puzis L, Koniaris LG, and Zimmers TA, (2012). JAK/STAT3 pathway inhibition blocks skeletal muscle wasting downstream of IL-6 and in experimental cancer cachexia. Am. J. Physiol. Endocrinol. Metab303, E410–E421. [PubMed: 22669242]

Del Campo A, Jaimovich E, and Tevy MF, (2016). Mitochondria in the aging muscles of flies and mice: new perspectives for old characters. Oxid. Med. Cell. Longev2016, 9057593. [PubMed: 27630760]

Fearon K, Arends J, and Baracos V, (2013). Understanding the mechanisms and treatment options in cancer cachexia. Nat. Rev. Clin. Oncol10, 90–99. [PubMed: 23207794]

Figueroa-Clarevega A, and Bilder D, (2015). Malignant Drosophila tumors interrupt insulin signaling to induce cachexia-like wasting. Dev. Cell33, 47–55. [PubMed: 25850672]

Flint TR, Janowitz T, Connell CM, Roberts EW, Denton AE, Coll AP, Jodrell DI, and Fearon DT, (2016). Tumor-induced IL-6 reprograms host metabolism to suppress anti-tumor immunity. Cell Metab. 24, 672–684. [PubMed: 27829137]

Herrera SC, and Bach EA, (2019). JAK/STAT signaling in stem cells and regeneration: from *Drosophila* to vertebrates. Development746, dev167643.

Hirata H, Tetsumoto S, Kijima T, Kida H, Kumagai T, Takahashi R, Otani Y, Inoue K, Kuhara H, Shimada K, et al. (2013). Favorable responses to tocilizumab in two patients with cancer-related cachexia. J. Pain Symptom Manage 46, e9–e13. [PubMed: 23602326]

Houtz P, Bonfini A, Liu X, Revah J, Guillou A, Poidevin M, Hens K, Huang HY, Deplancke B, Tsai YC, and Buchon N, (2017). Hippo, TGF-β, and Src-MAPK pathways regulate transcription of the upd3 cytokine in Drosophila enterocytes upon bacterial infection. PLoS Genet. 73, e1007091.

Huang K, Miao T, Chang K, Kim J, Kang P, Jiang Q, Simmonds AJ, Di Cara F, and Bai H, (2020). Impaired peroxisomal import in Drosophila oenocytes causes cardiac dysfunction by inducing upd3 as a peroxikine. Nat. Commun11, 2943. [PubMed: 32523050]

Jiang H, Patel PH, Kohlmaier A, Grenley MO, McEwen DG, and Edgar BA, (2009). Cytokine/Jak/Stat signaling mediates regeneration and homeostasis in the Drosophila midgut. Cell137, 1343–1355. [PubMed: 19563763]

Jorgensen SB, O'Neill HM, Sylow L, Honeyman J, Hewitt KA, Palanivel R, Fullerton MD, Öberg L, Balendran A, Galic S, et al. (2013). Deletion of skeletal muscle SOCS3 prevents insulin resistance in obesity. Diabetes 62, 56–64. [PubMed: 22961088]

Kandarian SC, Nosacka RL, Delitto AE, Judge AR, Judge SM, Ganey JD, Moreira JD, and Jackman RW, (2018). Tumour-derived leukaemia inhibitory factor is a major driver of cancer cachexia and morbidity in C26 tumour-bearing mice. J. Cachexia Sarcopenia Muscle9, 1109–1120. [PubMed: 30270531]

Katheder NS, Khezri R, O'Farrell F, Schultz SW, Jain A, Rahman MM, Schink KO, Theodossiou TA, Johansen T, Juhász G, et al. (2017). Microenvironmental autophagy promotes tumour growth. Nature 541, 417–420. [PubMed: 28077876]

Kierdorf K, Hersperger F, Sharrock J, Vincent CM, Ustaoglu P, Dou J, Gyoergy A, Groß O, Siekhaus DE, and Dionne MS, (2020). Muscle function and homeostasis require cytokine inhibition of AKT activity in Drosophila. eLife9, e51595. [PubMed: 31944178]

Kir S, White JP, Kleiner S, Kazak L, Cohen P, Baracos VE, and Spiegelman BM, (2014).Tumour-derived PTH-related protein triggers adipose tissue browning and cancer cachexia. Nature573, 100–104.

Kwon Y, Song W, Droujinine IA, Hu Y, Asara JM, and Perrimon N, (2015). Systemic organ wasting induced by localized expression of the secreted insulin/IGF antagonist ImpL2. Dev. Cell33, 36–46. [PubMed: 25850671]

Laird BJ, McMillan D, Skipworth RJE, Fallon MT, Paval DR, McNeish I, and Gallagher IJ, (2021). The emerging role of interleukin 1β (IL-1β) in cancer cachexia. Inflammation44, 1223–1228. [PubMed: 33907915]

Lee J, Ng KG, Dombek KM, Eom DS, and Kwon YV, (2021). Tumors overcome the action of the wasting factor ImpL2 by locally elevating Wnt/Wingless. Proc. Natl. Acad. Sci. USA778, e2020120118.

Markstein M, Dettorre S, Cho J, Neumüller RA, Craig-Müller S, and Perrimon N, (2014). Systematic screen of chemotherapeutics in Drosophila stem cell tumors. Proc. Natl. Acad. Sci. USA111, 4530–535. [PubMed: 24616500]

McEwen DG, and Peifer M, (2005). Puckered, a Drosophila MAPK phosphatase, ensures cell viability by antagonizing JNK-induced apoptosis. Development132, 3935–3946. [PubMed: 16079158]

Newton H, Wang YF, Camplese L, Mokochinski JB, Kramer HB, Brown AEX, Fets L, and Hirabayashi S, (2020). Systemic muscle wasting and coordinated tumour response drive tumourigenesis. Nat. Commun11, 4653. [PubMed: 32938923]

Nie Y, Yu S, Li Q, Nirala NK, Amcheslavsky A, Edwards YJK, Shum PW, Jiang Z, Wang W, Zhang B, et al. (2019). Oncogenic pathways and loss of the Rab11 GTPase synergize to alter metabolism in Drosophila. Genetics 212, 1227–1239. [PubMed: 31213502]

Owusu-Ansah E, Song W, and Perrimon N, (2013). Muscle mitohormesis promotes longevity via systemic repression of insulin signaling. Cell155, 699–712. [PubMed: 24243023]

Ren F, Wang B, Yue T, Yun EY, Ip YT, and Jiang J, (2010). Hippo signaling regulates Drosophila intestinestem cell proliferation through multiple pathways. Proc. Natl. Acad. Sci. USA107, 21064–21069. [PubMed: 21078993]

Sala D, and Sacco A, (2016). Signal transducer and activator of transcription 3 signaling as a potential target to treat muscle wasting diseases. Curr. Opin. Clin. Nutr. Metab. Care19, 171–176. [PubMed: 27023048]

Shaw RL, Kohlmaier A, Polesello C, Veelken C, Edgar BA, and Tapon N, (2010). The Hippo pathway regulates intestinal stem cell proliferation during Drosophila adult midgut regeneration. Development137, 4147–4158. [PubMed: 21068063]

Shin M, Cha N, Koranteng F, Cho B, and Shim J, (2020). Subpopulation of macrophage-like plasmatocytes attenuates systemic growth via JAK/STAT in the *Drosophila* fat body. Front. Immunol11, 63. [PubMed: 32082322]

Sloth Andersen A, Hertz Hansen P, Schaffer L, and Kristensen C, (2000). A new secreted insect protein belonging to the immunoglobulin superfamily binds insulin and related peptides and inhibits their activities. J. Biol. Chem275, 16948–16953. [PubMed: 10748036]

Song W, Ren D, Li W, Jiang L, Cho KW, Huang P, Fan C, Song Y, Liu Y, and Rui L, (2010). SH2B regulation of growth, metabolism, and longevity in both insects and mammals. Cell Metab. 11, 427–437. [PubMed: 20417156]

Song W, Veenstra JA, and Perrimon N, (2014). Control of lipid metabolism by tachykinin in Drosophila. Cell Rep. 9, 40–47. [PubMed: 25263556]

Song W, Cheng D, Hong S, Sappe B, Hu Y, Wei N, Zhu C, O'Connor MB, Pissios P, and Perrimon N, (2017a). Midgut-derived activin regulates glucagon-like action in the fat body and glycemic control. Cell Metab. 25, 386–399. [PubMed: 28178568]

Song W, Owusu-Ansah E, Hu Y, Cheng D, Ni X, Zirin J, and Perrimon N, (2017b). Activin signaling mediates muscle-to-adipose communication in a mitochondria dysfunction-associated obesity model. Proc. Natl. Acad. Sci. U S A114, 8596–8601. [PubMed: 28739899]

Song W, Kir S, Hong S, Hu Y, Wang X, Binari R, Tang HW, Chung V, Banks AS, Spiegelman B, and Perrimon N, (2019). Tumor-derived ligands trigger tumor growth and host wasting via differential MEK activation. Dev. Cell48, 277–286.e6. [PubMed: 30639055]

Staley BK, and Irvine KD, (2010).Warts and Yorkie mediate intestinal regeneration by influencing stem cell proliferation. Curr. Biol20, 1580–1587. [PubMed: 20727758]

Stec W, Vidal O, and Zeidler MP, (2013). Drosophila SOCS36E negatively regulates JAK/STAT pathway signaling via two separable mechanisms. Mol. Biol. Cell24, 3000–3009. [PubMed: 23885117]

Strassmann G, Fong M, Kenney JS, and Jacob CO, (1992). Evidence for the involvement of interleukin 6 in experimental cancer cachexia. J. Clin. Invest89, 1681–1684. [PubMed: 1569207]

Terry NA,Tulina N, Matunis E, and DiNardo S, (2006). Novel regulators revealed by profiling Drosophila testis stem cells within their niche. Dev. Biol294, 246–257. [PubMed: 16616121]

Thomas S, Fisher KH, Snowden JA, Danson SJ, Brown S, and Zeidler MP, (2015). Methotrexate is a JAK/STAT pathway inhibitor. PLoS ONE10, e0130078. [PubMed: 26131691]

Woodcock KJ, Kierdorf K, Pouchelon CA, Vivancos V, Dionne MS, and Geissmann F, (2015). Macrophage-derived upd3 cytokine causes impaired glucose homeostasis and reduced lifespan in Drosophila fed a lipid-rich diet. Immunity42, 133–144. [PubMed: 25601202]

Zhang G, Liu Z, Ding H, Zhou Y, Doan HA, Sin KWT, Zhu ZJ, Flores R, Wen Y, Gong X, et al. (2017). Tumor induces muscle wasting in mice through releasing extracellular Hsp70 and Hsp90. Nat. Commun 8, 589 [PubMed: 28928431]

Zhou X, Wang JL, Lu J, Song Y, Kwak KS, Jiao Q, Rosenfeld R, Chen Q, Boone T, Simonet WS, et al. (2010). Reversal of cancer cachexia and muscle wasting by ActRIIB antagonism leads to prolonged survival. Cell 142, 531–543. [PubMed: 20723755]

Highlights

- *yki*^{3SA}-gut tumors produce Upd3 to autonomously promote self-growth

- *yki*^{3SA}-gut tumors produce Upd3 to cause host wasting

- Upd3/Jak/Stat axis impairs muscle mitochondrial functions and carbolipid metabolism

- Upd3/Jak/Stat axis induces host ImpL2 production to hamper insulin response
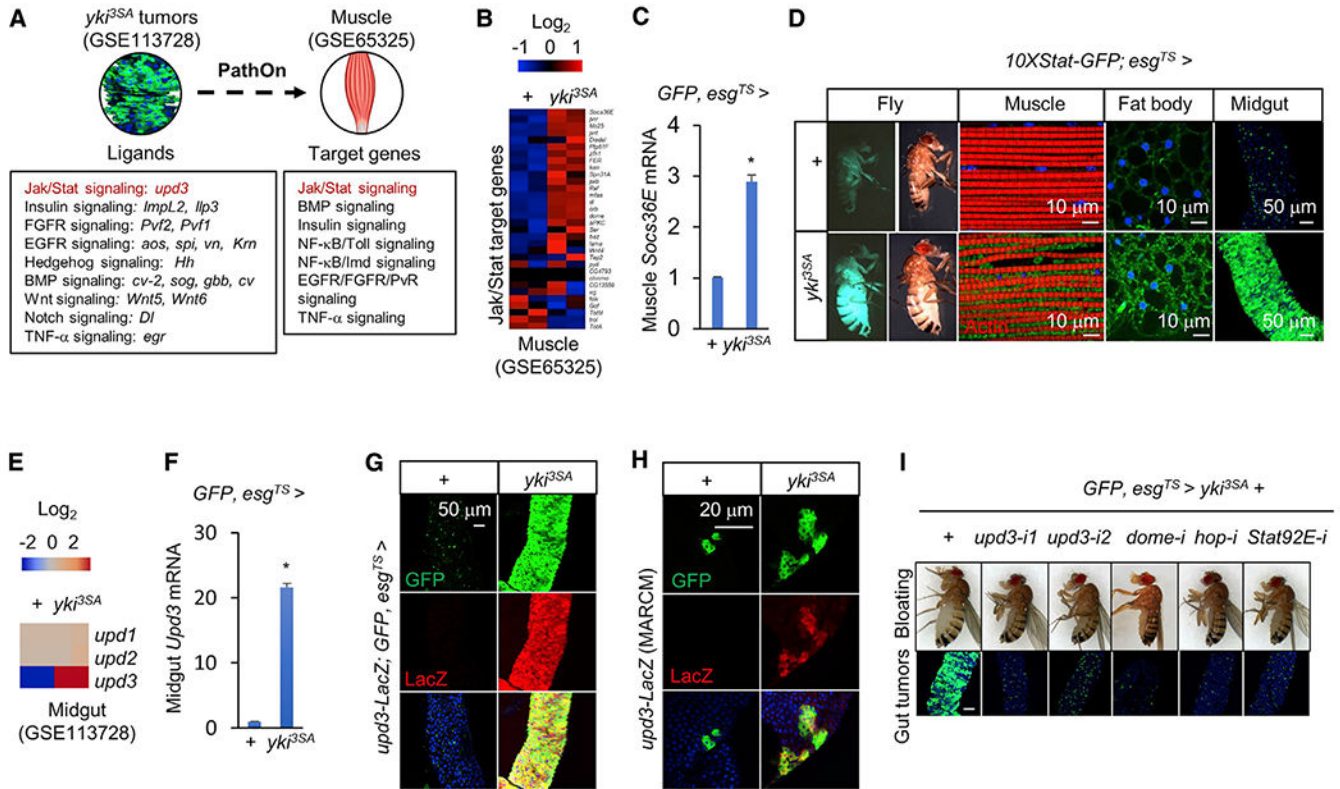
Figure 1. Upd3/Jak/Stat signaling is involved in tumor-host interactions

(A) Results of analysis with PathON, a software resource covering 14 canonical signaling pathways in *Drosophila*, reveal transcriptional changes in ligands and signature target genes of the indicated signaling pathways in gut tumors and muscles of *yki³ˢᴬ*-tumor-bearing flies, respectively, at day 8.

(B and C) Expression levels of target genes of Jak/Stat signaling in the muscles of control flies (+: *esg-GAL4, UAS-GFP, tub-GAL80^{TS}/+*) or *yki³ˢᴬ*-tumor-bearing flies (*yki³ˢᴬ: esg-GAL4, UAS-GFP, tub-GAL80^{TS}/+; UAS-yki³ˢᴬ/+*) at day 8. (B) Heatmap generated from GSE65325 RNA-seq data. (C) qPCR results (n = 3,5 flies/replicate).

(D) 10XStat-GFP signals in the muscle, fat body, midgut, and whole fly. Scale bars: muscle, fat body, 10 μm; midgut, 50 μm.

(E–G) Expression levels of Upd ligands in the midguts of control (+) and *yki³ˢᴬ*-tumor-bearing flies (*yki³ˢᴬ*) at day 8. (E) Heatmap generated from GSE113728 RNA-seq data.

(F) qPCR results (n = 3, 10 flies/replicate). (G) Immunostaining indicating Upd3-LacZ expression (green) in the midgut. Scale bar: 50 μm.

(H) MARCM assays indicating that *upd3-LacZ* expression (red) is increased mainly in the *yki*-tumor cells (green) and marginally in other gut cells. Scale bar: 20 μm.

(I) Changes in the bloating phenotype (top) and gut tumors (bottom) of indicated genotypes at day 8. Scale bar: 50 μm.

Data are presented as mean ± SEM. *p < 0.05.
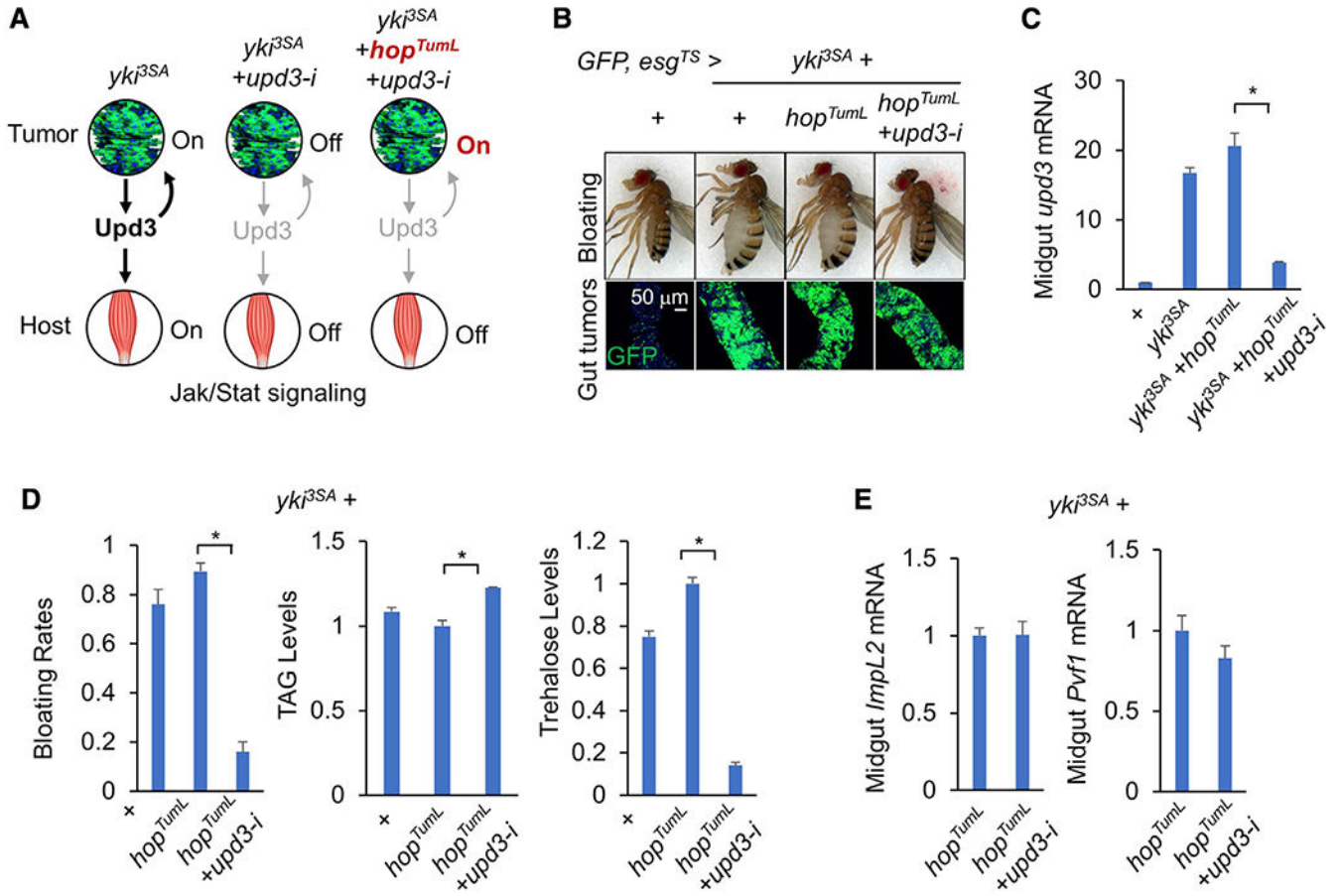
Figure 2. Tumor-produced Upd3 causes bloating and muscle dysfunction

(A) Experimental strategy for uncoupling Jak/Stat signaling in the tumors and host organs.

(B–D) Wasting effects in flies bearing $yki^{3SA}+hop^{TumL}$ tumors with $upd3$ RNAi
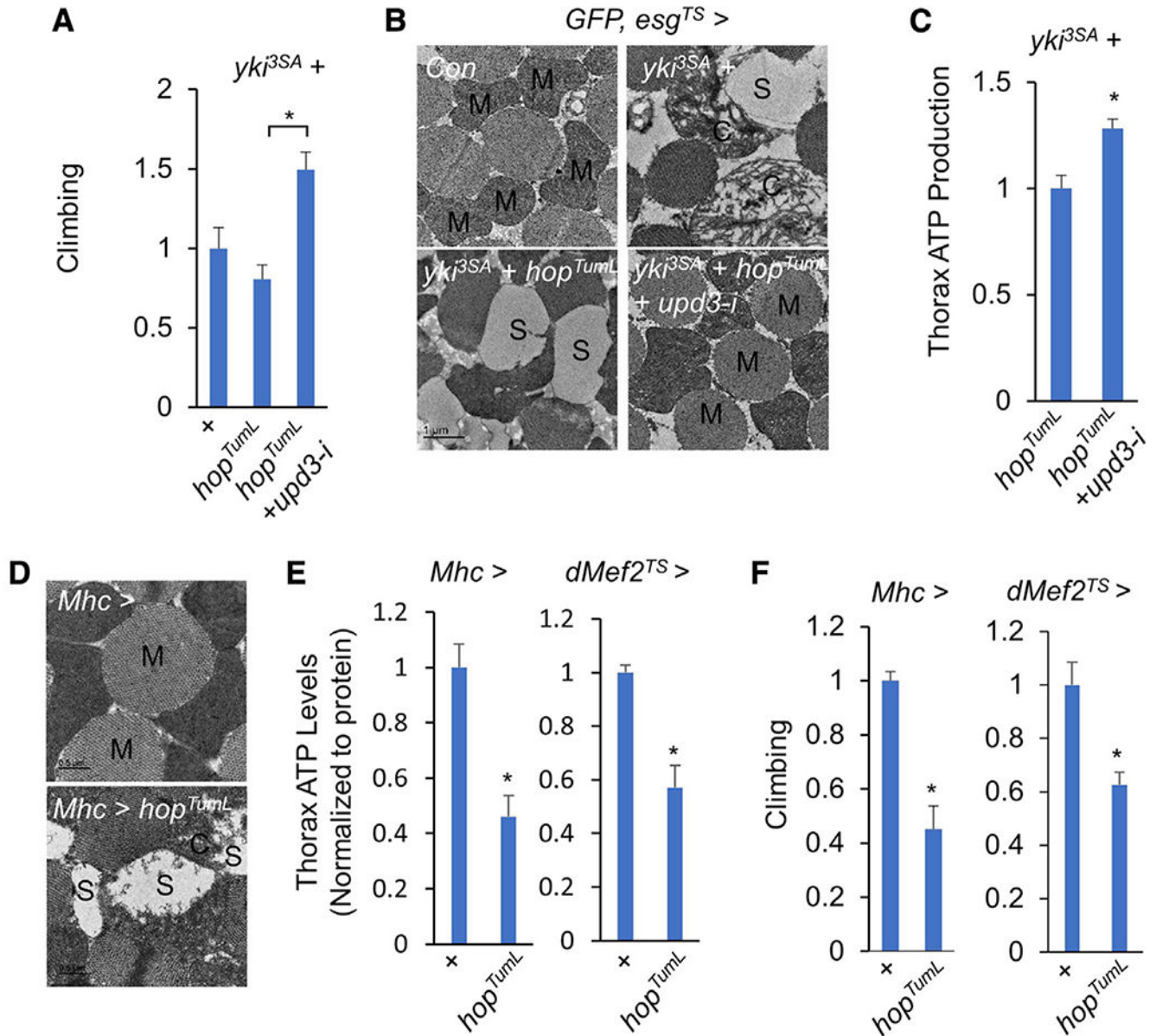
(HMS00646) at day 6: (B) bloating phenotype (top) and gut tumors (bottom; scale bar:

50 μm), (C) midgut gene expression of $upd3$ (n = 3, 10 flies/replicate), and (D) bloating rates

(n = 4, 20 flies/replicate) and TAG and trehalose levels (n = 3, 5 flies/replicate).

(E) Midgut gene expression of $ImpL2$ and $Pvf1$ (n = 3, 10 flies/replicate).

Data are presented as mean ± SEM. *p < 0.05.

Figure 3. Upd3/Jak/Stat signaling impairs muscle mitochondrial homeostasis

(A–C) Climbing rates (A; n = 15), muscle mitochondrial morphologies (scale bar: 1 μm) (B), and ATP production (C; n = 3, 5 flies/replicate) of flies bearing $yki^{3SA}+hop^{TumL}$ tumors with or without $upd3$ RNAi (HMS00646) at day 6.

(D–F) Muscle mitochondrial morphologies including normal mitochondria (M) and injured mitochondria with fragmented cristae (C) or blank space (S) (D; scale bar: 0.5 μm), ATP production (E; n = 3, 5 flies/replicate), and climbing rates (F; n = 15) of flies with activation of Jak/Stat signaling in the muscle at day 4.

Data are presented as mean ± SEM. *p < 0.05.
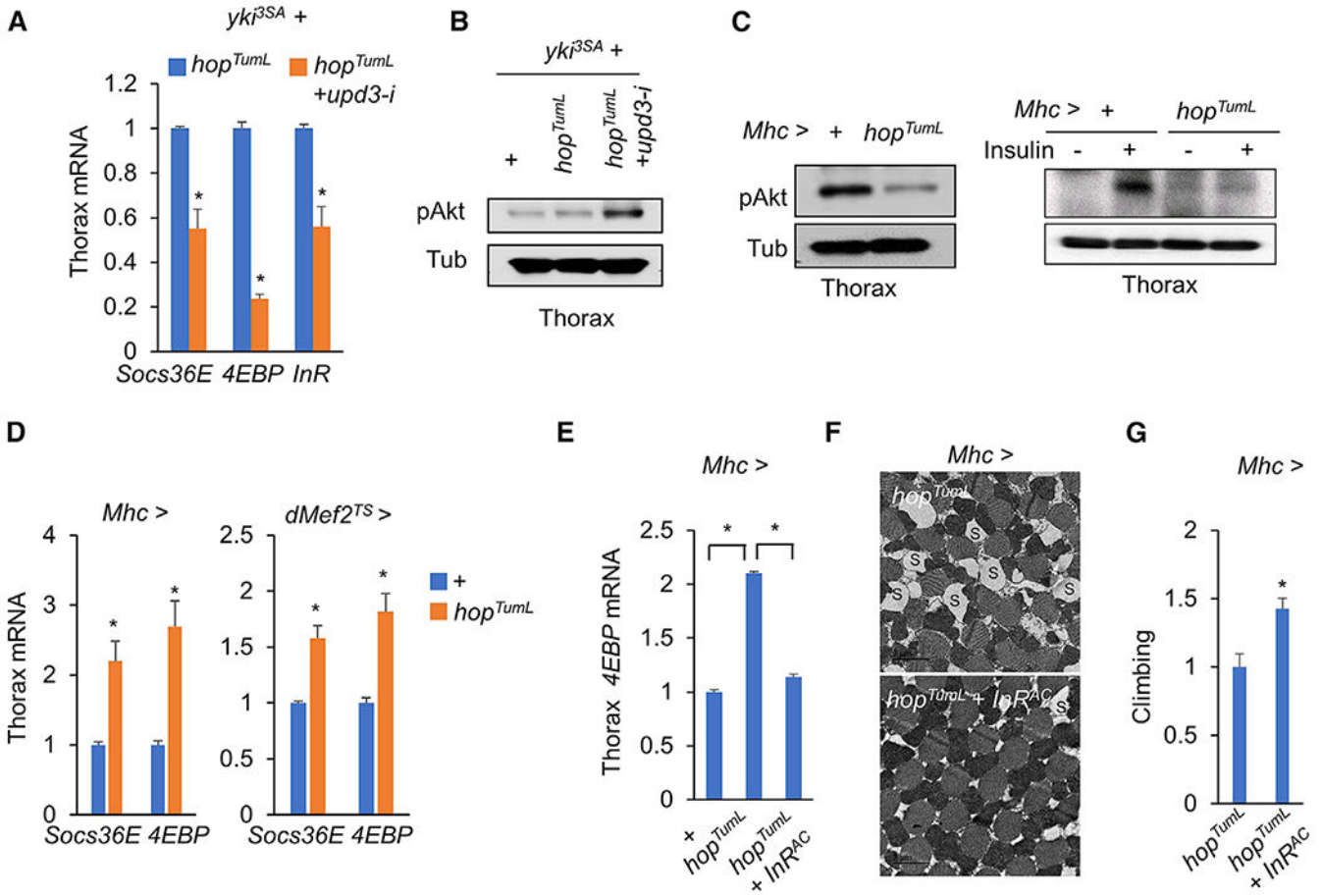
Figure 4. Upd3/Jak/Stat signaling impairs muscle insulin responses

(A and B) Insulin signaling, as indicated by target gene expression (A; n = 3,5 flies/ replicate) or p-Akt (B), in thethoraces of flies bearing yki^{3SA}-gut tumors with or without $upd3$ RNAi (HMS00646) at day 6.

(C and D) Insulin response, as indicated by p-Akt (C; left, freshly isolated thoraces; right, isolated thoraces that were treated with 1 μg/mL insulin for 30 min) or target gene expression (D; n = 3, 5 flies/replicate), in adult thoraces with activation of Jak/Stat signaling at day 4.

(E–G) Muscle gene expression (E; n = 3, 5 flies/replicate), muscle mitochondrial morphology including injured mitochondria with blank space (S) (scale bar: 2 μm) (F), and climbing rates (G; n = 15) of adult flies with activation of Jak/Stat and insulin signaling in the muscle at day 4.

Data are presented as mean ± SEM. *p < 0.05.

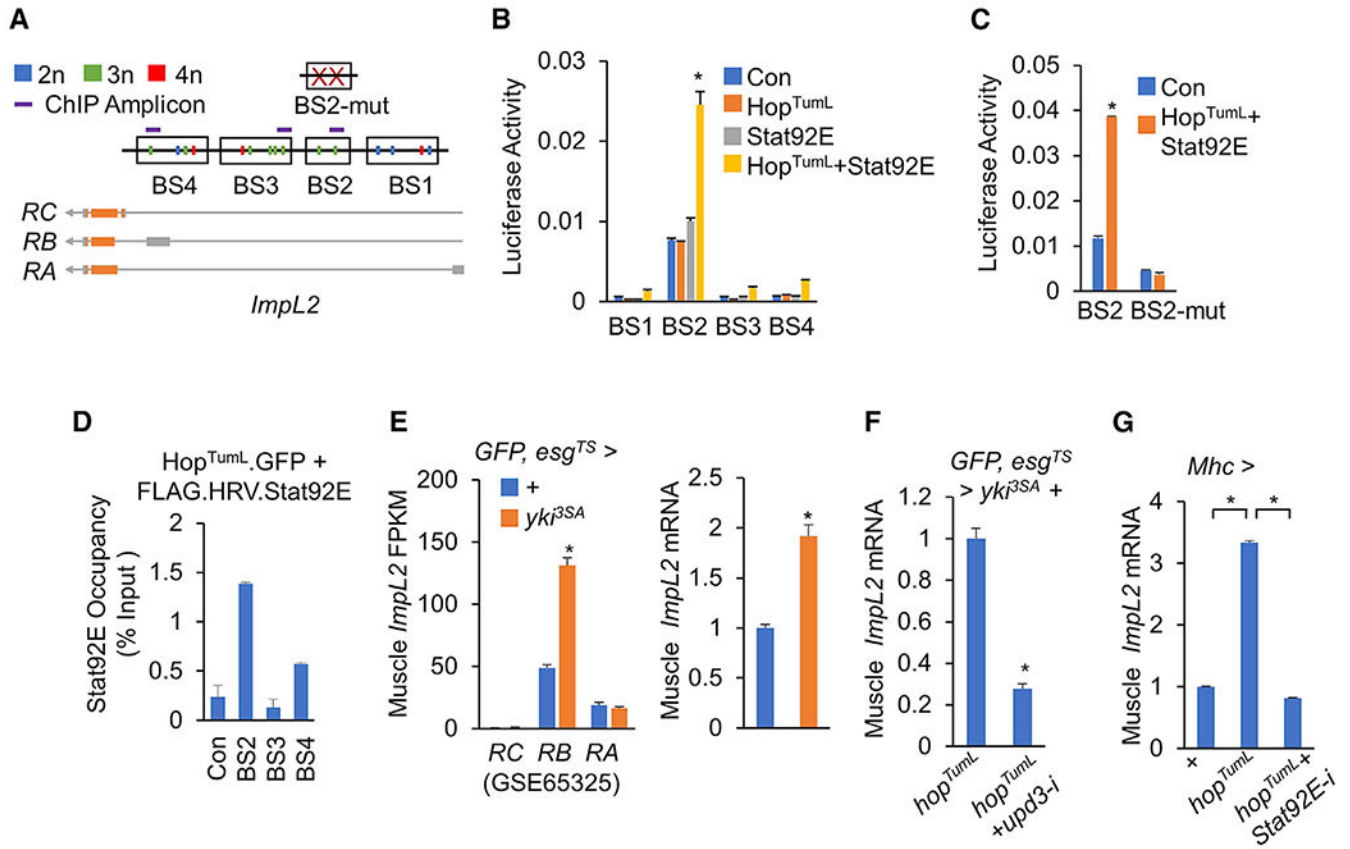**Figure 5. Upd3/Jak/Stat signaling promotes muscle *ImpL2* expression**

(A) Regions that contain putative Stat92E-binding sites (BS1-4) (TTCNNGAA, 2n, blue; TTCNNNGAA, 3n, green; TTCNNNNGAA, 4n, red) in the *ImpL2* gene, BS2 with two mutated Stat-binding sites (BS2-mut), and ChIP amplicons are shown.

(B and C) Relative luciferase activities of the indicated vectors that contain normal (B; BS1–4) and mutated (C; BS2-mut) Stat92E binding sites with Stat92E and/or Hop^{TumL} expression in S2R$^+$ cells (n = 3).

(D) The S2R$^+$ cells were transfected with indicated vector were lysed and pulled down with anti-FLAG antibody to perform *in vitro* ChIP assays. Stat92E occupancies at promoter regions of *ImpL2* as indicated relative to input were analyzed using qPCR. All ChIP-qPCR experiments were performed in duplicate.

(E) Expression levels of *ImpL2* in thoraces of flies bearing *yki^{3SA}*-gut tumors at day 8 from RNA-seq analysis (left; GSE65325, NCBI-GEO) and qPCR (right; n = 3, 5 flies/replicate).

(F and G) Muscle *ImpL2* expression levels of flies bearing tumors with or without *upd3* RNAi (HMS00646) at day 6 (F) or flies bearing *hop^{TumL}* overexpression with or without *Stat92E* RNAi in the muscle at day 6 (G) (n = 3, 5 flies/replicate).

Data are presented as mean ± SEM. *p < 0.05.

Figure 6. Jak/Stat signaling promotes organ wasting via ImpL2

(A–C) Thorax gene expression (A; n = 3, 5 flies/replicate), muscle mitochondrial morphology including injured mitochondria with blank space (S) (scale bar: 1 μm) (B), and climbing rates (C), n = 15) of flies with activation of Jak/Stat signaling plus *ImpL2* RNAi (NIG 15009R-3) in the muscle at day 6.

(D–F) Gene expression in abdomens (D; n = 3, 5 flies/replicate), whole-body TAG and trehalose levels (E; n = 3, 5 flies/replicate), abdomen appearance (F, top), and BODIPY that labels lipid droplets in the abdominal fat body (F, bottom; green, BODIPY; blue, DAPI; scale bar: 20 μm) of flies with activation of Jak/Stat signaling plus *ImpL2* RNAi (HMC05809) in the fat body at day 4

Data are presented as mean ± SEM. *p < 0.05.

Figure 7. Upd3 overexpression in the ISCs causes tumor formation and host wasting

(A–D) Fly appearance (A, top), gut tumors (A bottom; scale bar: 50 μm), thoracic muscle gene expression (B; n = 3, 5 flies/replicate), and wasting effects such as muscle mitochondrial morphology including injured mitochondria with blank space (S) (C; scale bar: 1 μm), TAG and Trehalose storages (D; n = 3, 5 flies/replicate), and climbing rates (D; n = 15) of adult flies with *upd3* overexpression in the ISCs at day 8. Data are presented as mean ± SEM. *p < 0.05

(E) Tumor-derived Upd3 coordinates tumor growth and host wasting via Jak/Stat signaling.

KEY RESOURCES TABLE

REAGENT or RESOURCE	SOURCE	IDENTIFIER
Antibodies		
Rabbit anti-phosphor-Akt (Ser473)	Cell Signaling	Cat#4060, RRID:AB_2315049
Mouse anti-α-tubulin	Sigma	Cat#T5168,RRID:AB_477579
Mouse anti-polyubiquitin (FK2)	Enzo	Cat#BML-PW8810,RRID:AB_10541840
Mouse anti-β-Gal	Promega	Cat#Z3781,RRID:AB_430877
Goat Anti-Mouse IgG (H+L), HRP	ABclonal	Cat#AS003, RRID:AB_2769851
Goat Anti-Rabbit IgG (H+L), HRP	ABclonal	Cat#AS014, RRID:AB_2769854
Goat anti-Mouse IgG (H+L) Highly Cross-Adsorbed Secondary Antibody, Alexa Fluor Plus 594	Thermo Fisher Scientific	Cat#A32742, RRID:AB_2762825
Rabbit monoclonal anti-FLAG	Genscript	Cat#A01868
Bacterial and virus strains		
DH5α Competent E.coli Strain	Vazyme	Cat#C502
Chemicals, peptides, and recombinant proteins		
Bradford Reagent	Sigma	Cat#B6916-500ML
Glycerol standard	Sigma	Cat#G7793-5ML
D-(+)-Glucose	Sigma	Cat#G7021
Trehalase	Sigma	Cat#E-TREH
Glucose assay reagent	Megazyme	Cat#K-Gluc
Triglyceride reagent	Sigma	Cat#T2449-10ML
Free glycerol reagent	Sigma	Cat#F6428-40ML
Glycerol	Sigma	Cat#G7793
Trizol	Thermo Fisher Scientific	Cat#15596018
HiScript II Q RT Supermix	Vazyme	Cat#R222-01
SYBR qPCR Master Mix	Vazyme	Cat#Q311-03
DAPI	Thermo Fisher Scientific	Cat#D1306
Bodipy 493/503	Thermo Fisher Scientific	Cat#D3922
Phalloidin	Thermo Fisher Scientific	Cat#A12381,
Insulin	Sigma	Cat#I6634
Methotrexate	Selleck	Cat#S1210
Critical commercial assays		
CellTiter-LumiTM Plus kit	Beyotime	Cat#C0068M
Trehalose Assay Kit	Megazyme	Cat#K-Gluc
Triglyceride Assay Kit	Sigma	Cat#T2449
Effectene reagent	QIAGEN	Cat#301425
Pierce Protein A/G Magnetic Beads	Thermo Fisher Scientific	Cat#88803
ClonExpress MultiS One Step Cloning Kit	Vazyme	Cat#C113-01
HRV 3C Protease	TaKaRa	Cat#7360-1
Dual-Luciferase Reporter assay kit	Promega	Cat#E1910

REAGENT or RESOURCE	SOURCE	IDENTIFIER
Antibodies		
Deposited data		
RNaseq data from fly midgut	(Kwon et al., 2015)	GEO: GSE113728
RNaseq data from fly muscle	(Song et al., 2019)	GEO: GSE65325
Experimental models: Cell lines		
D. melanogaster: Cell line S2R$^+$	Laboratory of Norbert Perrimon, Harvard Medical School	N/A
D.melanogaster: esg-GAL4, tub-GAL80^{TS}, UAS-GFP	(Kwon et al., 2015)	N/A
D.melanogaster: Myo1A-GAL4, esg-GAL4, tub-GAL80^{TS}	(Song et al., 2019)	N/A
D.melanogaster: CG-GAL4, tub-GAL80^{TS}	(Song et al., 2017b)	N/A
D.melanogaster: tub-GAL80^{TS}, Lpp-GAL4	(Song et al., 2017b)	N/A
D.melanogaster: tub-GAL80^{TS}, dMef2-GAL4	(Owusu-Ansah et al., 2013)	N/A
D.melanogaster: tub-GAL80^{TS}, Mhc-GAL4	(Owusu-Ansah et al., 2013)	N/A
D.melanogaster: 10XStat-GFP	(Bach et al., 2007)	N/A
D.melanogaster: UAS-Pvf1	(Song et al., 2019)	N/A
D.melanogaster: UAS-hop^{TumL}	A gift from Dr. Erika Bach, NYU Langone Health	N/A
D.melanogaster: UAS-upd3	A gift from Dr. Bruce Edgar, University of Utah	N/A
D.melanogaster: upd3-lacZ	A gift from Dr. Bruce Edgar, University of Utah	N/A
D.melanogaster: FRT19A	A gift from Dr. Zheng Guo, Huazhong University of Science and Technology	N/A
D.melanogaster: yw, hs-FLP, tub-GAL80, FRT19A; UAS-GFP	A gift from Dr. Zheng Guo, Huazhong University of Science and Technology	N/A
D.melanogaster: UAS-Stat92E-RNAi	A gift from Drs. Xinhua Lin and Yun Qi, Fudan University	N/A
D.melanogaster: UAS-upd3-RNAi1	TRiP at Harvard Medical School	HMS000646
D.melanogaster: UAS-upd3-RNAi2	TRiP at Harvard Medical School	HMS05061
D.melanogaster: UAS-hop-RNAi	TRiP at Harvard Medical School	HMS00761
D.melanogaster: UAS-Stat92E-RNAi	TRiP at Harvard Medical School	HMS00035
D.melanogaster: UAS-ImpL2-RNAi	TRiP at Harvard Medical School	HMS05891
D.melanogaster: UAS-w-RNAi	TRiP at Harvard Medical School	HMS01545
D.melanogaster: w^{1118}	Bloomington Stock Center	BDSC_3605
D.melanogaster: upd3	Bloomington Stock Center	BDSC_55728
D.melanogaster: USA-yki^{3SA}	Bloomington Stock Center	BDSC_28817
D.melanogaster: USA-InR^{AC}	Bloomington Stock Center	BDSC_8248
D.melanogaster: UAS-ImpL2-RNAi	National Institute of Genetics	15009R-3
D.melanogaster: UAS-dome-RNAi	Vienna Drosophila Resource Center	v19717
Oligonucleotides		

REAGENT or RESOURCE	SOURCE	IDENTIFIER
Antibodies		
See Table S4 for oligonucleotide information		N/A
Recombinant DNA		
pAc5.1	Thermo Fisher Scientific	Cat#V411020
pGL3-Basic	Promega	Cat#E1751
pAc5-Stat92E-RB	This paper	N/A
pAc5-hop^{TumL}	This paper	N/A
pGL3-hsp70	This paper	N/A
pGL3-ImpL2-BS1	This paper	N/A
pGL3-ImpL2-BS2	This paper	N/A
pGL3-ImpL2-BS3	This paper	N/A
pGL3-ImpL2-BS4	This paper	N/A
pGL3-ImpL2-BS2-mut	This paper	N/A
pAc-HRV.FLAG.Stat92E.RB-T2A-hop^{TumL}-GFP	This paper	N/A
Software and algorithms		
ImageJ	NIH	https://imagej.nih.gov/ij/download.html
Microsoft Excel	Microsoft	https://www.microsoft.com/en-us/microsoft-365/excel
Other		
QSonica sonicator	QSonica	#Q125 system
Multi-sample tissuelyser-24	Shanghai Jingxin Technology	N/A
Nikon SMZ18	Nikon	N/A
Nikon Eclipse Ts2	Nikon	N/A
Zeiss LSM880	Zeiss	N/A
CFX96 Real-Time System/C1000 Thermal Cycler	Bio-Rad	N/A